Characterization of Range Sidelobe Modulation Arising from Radar-Embedded Communications

Cenk Sahin[1], Justin G. Metcalf[1], and Shannon D. Blunt[2]
[1] Sensors Directorate, Air Force Research Laboratory, Wright-Patterson Air Force Base, OH
[2] Department of Electrical Engineering & Computer Science, University of Kansas, Lawrence, KS

***Abstract*—When information sequences are embedded into radar waveforms by means of coding diversity, the resulting radar emissions then change on a pulse-to-pulse basis during a coherent processing interval (CPI). As such, pulse compression of these different waveforms leads to different sidelobe structures, giving rise to range sidelobe modulation (RSM) of the clutter. The presence of RSM induces a partial loss of coherency after Doppler processing, resulting in residual clutter after cancellation, and hence reduced target visibility.**

Here the RSM effect is mathematically characterized within a phase-modulated radar-embedded communication framework. A closed-form expression for the expected value of the residual clutter power, referred to as the RSM power, is derived. The RSM power is found to not be dependent on the Doppler frequency or time-bandwidth product, but is a decreasing function of the number of pulses in the CPI and an increasing function of the modulation index. The latter controls the amount of phase shift within the radar pulse due to each communication symbol.

I. Introduction

With the demand for radio spectrum by commercial communication applications increasing exponentially, radar sensing applications continue to lose spectrum while striving to maintain legacy capabilities [1]. As such, ongoing research is focused on developing methods to share spectrum between multiple functions (e.g. radar and communications [2]). The notion of radar/communication spectrum sharing necessitates the use of some manner of waveform diversity [3]–[5] through the exploitation of available time, frequency, coding, spatial, or polarization degrees-of-freedom [6]–[17]. Here we examine the use of coding in the fast-time domain in which the radar waveform is further modulated to include communication information [6]–[9], [18]. From a radar perspective, the result of this coding operation is that the structure of the radar emission is now time-varying.

The primary challenge with varying the radar emission from pulse to pulse within a coherent processing interval (CPI) is the clutter range sidelobe modulation (RSM) [6], [19]. The RSM arises because the pulse compression matched filtering (MF) of different radar-embedded communication (REC) waveforms leads to different sidelobe structures. When Doppler processing is performed across the CPI of pulsed echoes, the presence of RSM induces a partial loss of coherency, the consequence of which is increased residual clutter after cancellation, and thus degraded target detection performance. It follows that RSM is a very important consideration in coding diversity REC system design, which has also recently been addressed by advanced receiver processing techniques [6], [18], [20]–[23]. A common feature among these techniques is a significant increase in computational complexity compared to the standard processing approach of a MF followed by discrete Fourier transform (DFT) Doppler processing (MF-DFT processing).

Despite recent efforts to remediate it, the RSM effect has not previously been mathematically characterized. Here we initiate a mathematical treatment of RSM for REC systems where phase-modulated radar and communication waveforms are combined via [7] to form phase-modulated composite emissions. The motivation for focusing on phase-modulated emissions is the polyphase-coded FM (PCFM)-based [24] REC formulation introduced in [7]. With this approach, communication symbols are embedded into radar emissions under constant envelope constraints in a continuous phase modulation (CPM) [25] framework. This arrangement produces joint radar/communication emissions that are constant amplitude and well-contained spectrally, thus ensuring they are amenable to high-power transmitters [24]. In addition, the approach in [7] allows for control of the degree of RSM by adjusting the *modulation index* to trade-off communication performance (namely, data throughput and bit error rate (BER)) for radar performance (clutter cancellation).

Because the CPM structure contains memory [25], the RSM effect is examined here within a phase-shift keying (PSK) [26] REC framework [8] using random biphase radar codes. This PSK structure is a special case of the more general PCFM-CPM radar/communication framework proposed in [7] and is used here, along with the assumption of a randomly coded radar waveform for each CPI, to facilitate a mathematically tractable analysis of the RSM. The results of this analysis subsequently provide greater understanding of RSM behavior for the more general (and physically realizable) PCFM-CPM structure. We derive a closed-form expression for the (average) RSM/residual clutter power after MF-DFT processing. This expression is a function of the modulation index, Doppler frequency, Doppler windowing function, time-bandwidth product, number of pulses in the CPI, and sampling rate. The closed-form nature of this expression provides insight into the design trade-offs inherent with REC systems. More importantly, it

This research was performed while Cenk Sahin held an NRC Research Associateship award at the Air Force Research Laboratory, Wright-Patterson AFB, OH. This work was supported in part by the Air Force Research Laboratory - Sensors Directorate, and by a subcontract with Matrix Research, Inc. for research sponsored by Air Force Research Laboratory under Prime Contract #FA8650-14-D-1722.

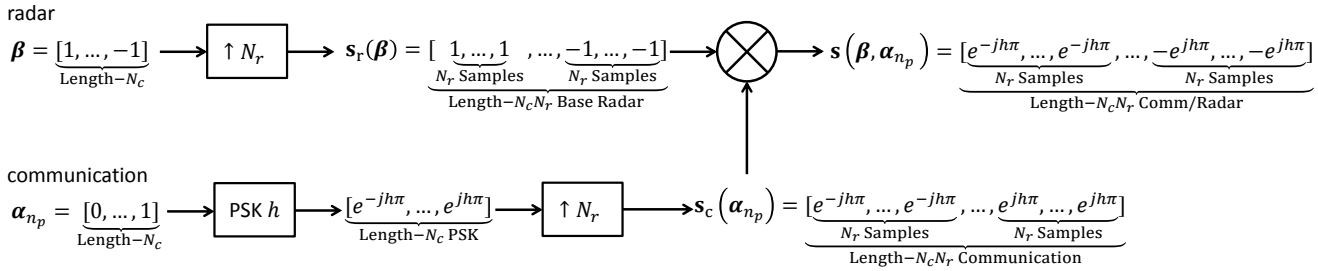

Fig. 1. Block diagram of discrete-time representation of PSK-based REC for the n_p-th pulse.

can be used to evaluate the performance of different design strategies and and to enable their selection based on the radar and communication performance requirements.

II. System Model

With the REC system under consideration, the emitted signal is the product of a radar waveform and a communication waveform [7], [8]. The *base radar waveform* is a polyphase-coded waveform that is constant during the CPI while the communication waveform is a phase-modulated communication sequence that varies from pulse to pulse. Thus the resulting (composite) REC waveform likewise changes on a pulse-to-pulse basis.

The REC waveform at the n_p-th pulse, for $n_p = 0, \cdots, N_p - 1$, with N_p the number of pulses in a CPI, is defined as the product

$$s_{n_p}(t; \boldsymbol{\beta}, \boldsymbol{\alpha}_{n_p}) = s_{\mathrm{r}}(t; \boldsymbol{\beta}) s_{\mathrm{c},n_p}(t; \boldsymbol{\alpha}_{n_p}), \tag{1}$$

where $s_{\mathrm{r}}(t; \boldsymbol{\beta})$ is the *base radar waveform* and $s_{\mathrm{c},n_p}(t; \boldsymbol{\alpha}_{n_p})$ is the communication waveform component. Since both $s_{\mathrm{r}}(t; \boldsymbol{\beta})$ and $s_{\mathrm{c},n_p}(t; \boldsymbol{\alpha}_{n_p})$ are phase-modulated, the product $s_{n_p}(t; \boldsymbol{\beta}, \boldsymbol{\alpha}_{n_p})$ is likewise phase-modulated. Here the code $\boldsymbol{\beta} = [\beta_0, \cdots, \beta_{N_c-1}]$, for N_c the number of chips per pulse (which closely approximates the time-bandwidth product), is a random biphase code, i.e. $\beta_{n_c} \in \{-1, +1\}$ for all $n_c = 0, \cdots, N_c - 1$, that changes independently from CPI to CPI, but remains the same during each CPI. The code values $\beta_{n_c}, n_c = 0, \cdots, N_c - 1$, are independent and identically distributed (i.i.d.) with -1 and $+1$ having equal probability. Therefore, the base radar waveform also changes on a CPI-to-CPI basis, with the random biphase code assumption invoked for the sake of mathematical tractability. On the other hand, the communication symbol sequence $\boldsymbol{\alpha}_{n_p}$, and therefore the communication waveform $s_{\mathrm{c},n_p}(t; \boldsymbol{\alpha}_{n_p})$, changes on a pulse-to-pulse basis. It therefore follows that the composite REC waveform $s_{n_p}(t; \boldsymbol{\beta}, \boldsymbol{\alpha}_{n_p})$ also changes on a pulse-to-pulse basis during the CPI.

A block diagram for an instantiation of the PSK-based REC for the n_p-th pulse in shown in Fig.1. The discrete-time representation of the base radar waveform, denoted as $\mathbf{s}_{\mathrm{r}}(\boldsymbol{\beta})$, is obtained by the 0-th order representation of $s_{\mathrm{r}}(t; \boldsymbol{\beta})$ (discrete codes with abrupt phase changes [27]) with N_r samples per chip, resulting in

$$\mathbf{s}_{\mathrm{r}}(\boldsymbol{\beta}) = [s_{\mathrm{r},0}(\boldsymbol{\beta}), \cdots, s_{\mathrm{r},N_cN_r-1}(\boldsymbol{\beta})], \tag{2}$$

where $\mathbf{s}_{\mathrm{r},n_cN_r+n_r}(\boldsymbol{\beta}) = \beta_{n_c}$ for all $n_c = 0, \cdots, N_c - 1$ and $n_r = 0, \cdots, N_r - 1$. The 0-th order code-based representation is likewise invoked for mathematical tractability of RSM analysis. The discrete-time representation of the composite waveform for the n_p-th pulse is therefore

$$\begin{aligned}\mathbf{s}_{n_p}(\boldsymbol{\beta}, \boldsymbol{\alpha}_{n_p}) = [&s_{\mathrm{r},0}(\boldsymbol{\beta}) s_{\mathrm{c},n_p,0}(\boldsymbol{\alpha}_{n_p}), \cdots \\ &, s_{\mathrm{r},N_cN_r-1}(\boldsymbol{\beta}) s_{\mathrm{c},n_p,N_cN_r-1}(\boldsymbol{\alpha}_{n_p})],\end{aligned} \tag{3}$$

where $\boldsymbol{s}_{\mathrm{c},n_p}(\boldsymbol{\alpha}_{n_p}) = [s_{\mathrm{c},n_p,0}(\boldsymbol{\alpha}_{n_p}), \cdots, s_{\mathrm{c},n_p,N_cN_r-1}(\boldsymbol{\alpha}_{n_p})]$ is the discrete-time representation of the communication component of the n_p-th pulse, which has the same length (in samples) as the discrete-time base radar waveform.

The communication symbol sequence $\boldsymbol{\alpha}_{n_p}$ is binary and the number of communication symbols is equal to the number of chips, i.e. $\boldsymbol{\alpha}_{n_p} = [\alpha_{n_p,0}, \cdots, \alpha_{n_p,N_c-1}]$ and $\alpha_{n_p,n_c} \in \{0, 1\}$ for $n_c = 0, \cdots, N_c - 1$. The communication sequences are modulated with PSK [26] having an adjustable phase-shift parameter [7], [8] referred to as the modulation index. The relationship between the communication symbols and samples of the discrete-time communication component is given as

$$s_{\mathrm{c},n_p,n_cN_r+n_r}(\boldsymbol{\alpha}_{n_p}) = \begin{cases} \exp\{-jh\pi\} & \text{if } \alpha_{n_p,n_c} = 0 \\ \exp\{jh\pi\} & \text{if } \alpha_{n_p,n_c} = 1, \end{cases} \tag{4}$$

for all $n_c = 0, \cdots, N_c - 1$, $n_r = 0, \cdots, N_r - 1$ and $n_p = 0, \cdots, N_p - 1$. The modulation index $\frac{1}{2} \geq h \geq 0$ is a rational number that controls the amount of phase shift introduced to the base radar waveform when embedding a communication symbol. As h is reduced the radar waveforms in a CPI become more similar, and in the limiting case of $h = 0$ all radar waveforms are identical since no communication takes place. The binary values α_{n_p,n_c} are i.i.d. In other words, α_{n_p,n_c} and α_{m_p,m_c} are independent whenever $n_p \neq m_p$ or $n_c \neq m_c$. It follows that the communication waveform segments $s_{\mathrm{c},n_p,n_cN_r+n_r}(\boldsymbol{\alpha}_{n_p})$ and $s_{\mathrm{c},m_p,m_cN_r+m_r}(\boldsymbol{\alpha}_{m_p})$ are independent for all $n_r, m_r = 0, \cdots, N_r - 1$ whenever $n_p \neq m_p$ or $n_c \neq m_c$. An interesting case for the PSK-based REC is with $h = \frac{1}{2}$, where the samples of the communication component given in (4), and hence the samples of the discrete-time REC waveforms, are drawn from $\{-j, j\}$. In this case, the discrete-time REC waveforms can be modeled as random biphase codes that change independently on a pulse-to-pulse basis with elements drawn i.i.d. from $\{-j, j\}$.

The PSK-based REC is considered here instead of the more complicated continuous phase constant envelope PCFM-based REC design in [7] for the purpose of mathematical tractability. Because of the memory of CPM, closed-form solutions are often either unobtainable or do not explicitly show the dependence on CPM parameters. The extension of this work to PCFM-based REC is a topic of ongoing investigation.

The clutter response for the n_p-th pulse repetition interval (PRI) is modeled as the convolution of a complex-valued white Gaussian random sequence, denoted as $\boldsymbol{\omega} = [\omega_{-N}, \cdots, \omega_0, \cdots, \omega_N]$, for $N \gg N_c N_r$, with the discrete-time representation of the n_p-th REC waveform $\mathbf{s}_{n_p}(\boldsymbol{\beta}, \boldsymbol{\alpha}_{n_p})$. Each random sample ω_n has variance σ_ω^2/N_r to ensure that σ_ω^2 is *the average clutter power per range bin*, which does not scale with the sampling rate N_r. The n-th clutter response sample for the n_p-th PRI denoted by $c_{n_p,n}(\boldsymbol{\omega}, \boldsymbol{\beta}, \boldsymbol{\alpha}_{n_p})$ is given, for $-N \leq n \leq N$, as

$$c_{n_p,n}(\boldsymbol{\omega}, \boldsymbol{\beta}, \boldsymbol{\alpha}_{n_p}) = \sum_{l=0}^{N_c N_r - 1} \omega_{n-l} s_{\mathrm{r},l}(\boldsymbol{\beta}) s_{\mathrm{c},n_p,l}(\boldsymbol{\alpha}_{n_p}). \quad (5)$$

This clutter response is dependent on $\boldsymbol{\beta}$, $\boldsymbol{\omega}$ and $\boldsymbol{\alpha}_{n_p}$. However, the Gaussian sequence $\boldsymbol{\omega}$ used to drive the clutter response remains constant within the CPI while the communication sequence $\boldsymbol{\alpha}_{n_p}$ varies from pulse to pulse. This modeling approach is based on the assumption that clutter does not appreciably change on a time scale smaller than the CPI, and that the radar platform is stationary. The impact of platform motion and internal clutter motion (ICM) are additional topics of ongoing investigation.

III. Range Sidelobe Modulation

In this section the average power of the clutter after MF-DFT processing is characterized. Because the random process $\boldsymbol{\omega}$ is stationary, the statistics of the clutter samples $c_{n_p,n}(\boldsymbol{\omega}, \boldsymbol{\beta}, \boldsymbol{\alpha}_{n_p})$ do not change within the PRI. Therefore, the subscript n can be dropped or simply set to $n = 0$. The clutter response after MF at the n_p-th PRI, denoted by $\widehat{c}_{n_p}(\boldsymbol{\omega}, \boldsymbol{\beta}, \boldsymbol{\alpha}_{n_p})$, can be written as

$$\widehat{c}_{n_p}(\boldsymbol{\omega}, \boldsymbol{\beta}, \boldsymbol{\alpha}_{n_p}) = \frac{1}{N_c N_r} \sum_{l=-N_c N_r+1}^{N_c N_r - 1} \omega_{-l} \sum_{i=0}^{N_c N_r - 1} s_{\mathrm{r},i} s^*_{\mathrm{r},i-l} s_{\mathrm{c},n_p,i}(\boldsymbol{\alpha}_{n_p}) s^*_{\mathrm{c},n_p,i-l}(\boldsymbol{\alpha}_{n_p}), \quad (6)$$

where $(\cdot)^*$ denotes complex conjugation, and the scaling by $\frac{1}{N_c N_r}$ is included for normalization. The expression (6) is the convolution of $\boldsymbol{\omega}$ and the autocorrelation of the discrete-time REC waveform $\mathbf{s}_{n_p}(\boldsymbol{\beta}, \boldsymbol{\alpha}_{n_p})$. When communication sequences are not embedded into radar emissions (i.e. $\mathbf{s}_{n_p}(\boldsymbol{\beta}, \boldsymbol{\alpha}_{n_p})$ is constant for all $n_p = 0, \cdots, N_p - 1$), the clutter response after MF does not vary from pulse to pulse (internal clutter motion not withstanding). However, within the REC framework the range sidelobe coherence across the CPI of MF outputs is lost, resulting in the range sidelobe modulation (RSM) effect [6], [19].

The average clutter power after MF-DFT processing with the Doppler windowing function $\boldsymbol{\Gamma} = [\Gamma_0, \cdots, \Gamma_{N_p-1}]$ for normalized Doppler frequency $-0.5 \leq \phi \leq 0.5$ is defined as

$$C_{\text{POWER}}(\phi, \boldsymbol{\Gamma}) = \mathbb{E}\left[\left| \sum_{n_p=0}^{N_p-1} \Gamma_{n_p} \widehat{c}_{n_p}(\boldsymbol{\omega}, \boldsymbol{\beta}, \boldsymbol{\alpha}_{n_p}) \exp\{-j2\pi\phi n_p\} \right|^2 \right], \quad (7)$$

where $\widehat{c}_{n_p}(\boldsymbol{\omega}, \boldsymbol{\beta}, \boldsymbol{\alpha}_{n_p})$ is given in (6), the windowing function is normalized such that $\sum_{n_p=1}^{N_p-1} \Gamma_{n_p} = 1$, and the expected value is computed with respect to $\boldsymbol{\omega}, \boldsymbol{\alpha}_0, \cdots, \boldsymbol{\alpha}_{N_p-1}$ and $\boldsymbol{\beta}$. For the REC formulation under consideration, it can be shown that the clutter power can written as the closed-form expression

$$C_{\text{POWER}}(\phi, \boldsymbol{\Gamma}, h, \sigma_\omega^2, N_p, N_c, N_r) = \sigma_\omega^2 \left(\frac{2}{3} + \frac{1}{3N_r^2} \right) \times \left[\sin^2(h\pi) \left(1 + \cos^2(h\pi) \right) \frac{N_c - 1}{N_c} \left(\sum_{n_p=0}^{N_p-1} \Gamma_{n_p}^2 \right) + \left(1 + \cos^4(h\pi) \frac{N_c - 1}{N_c} \right) \left| \mathrm{DFT}_{\boldsymbol{\Gamma}}(\phi) \right|^2 \right], \quad (8)$$

where $\mathrm{DFT}_{\boldsymbol{\Gamma}}(\phi) = \sum_{n_p=0}^{N_p-1} \Gamma_{n_p} \exp\{-j2\pi\phi n_p\}$ is the DFT of $\boldsymbol{\Gamma}$ computed at ϕ. Due to space constraints the proof of (8) is omitted here. In the derivation of (8), only the i.i.d. property of $\boldsymbol{\omega}$ is used while the Gaussian property is not. It follows that the clutter power expression is valid for any white random process model (i.e. zero-mean i.i.d. random samples) with σ_ω^2 representing the variance of the respective process. The first term inside the square brackets of (8) is due to the terms in the expected value expression of (7) that vary from pulse to pulse during the CPI; therefore, it quantifies the RSM effect and is referred to as the *RSM power*. The second term in (8) is due to the terms in (7) that remain constant during the CPI, and it is referred to as the *coherent clutter power*. It is important to note that the RSM power does not depend on the normalized Doppler frequency ϕ while the coherent clutter power does depend on ϕ through the DFT of the Doppler windowing function computed at ϕ.

The mainlobe of the range-Doppler response of the coherent clutter component is centered at $\phi = 0$, while its sidelobes decay as $|\phi|$ increases by a pattern and rate specified by the Doppler windowing function and number of pulses in the CPI. By the appropriate choice of the Doppler windowing function the coherent clutter power can be made arbitrarily small—compared to the RSM power—for Doppler frequency values greater than some threshold $\overline{\phi} > 0$. Therefore, the lower bound on the clutter power of the form

$$C_{\text{POWER}}(\phi, \boldsymbol{\Gamma}, h, \sigma_\omega^2, N_p, N_c, N_r) \geq \sigma_\omega^2 \left(\frac{2}{3} + \frac{1}{3N_r^2} \right) \times \sin^2(h\pi) \left(1 + \cos^2(h\pi) \right) \frac{N_c - 1}{N_c} \left(\sum_{n_p=0}^{N_p-1} \Gamma_{n_p}^2 \right) \quad (9)$$

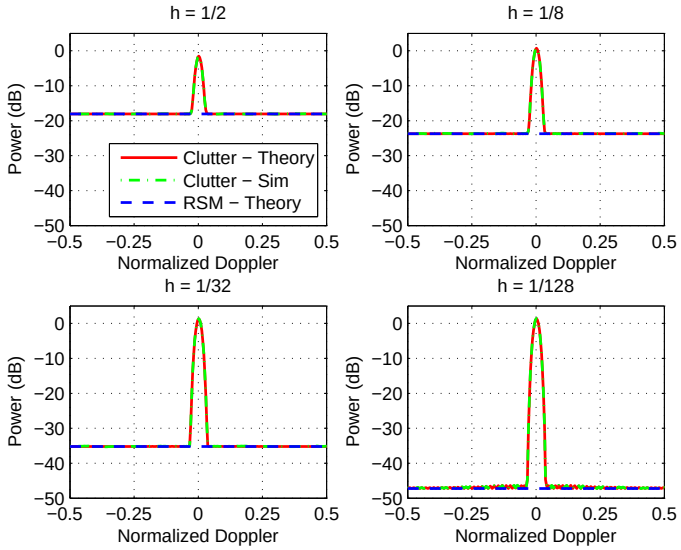

Fig. 2. Clutter power computed via (8), by simulation, and RSM power computed via (9) plotted as a function of the normalized Doppler frequency ϕ for modulation indices $h = \frac{1}{2}, \frac{1}{8}, \frac{1}{32}$ and $\frac{1}{128}$.

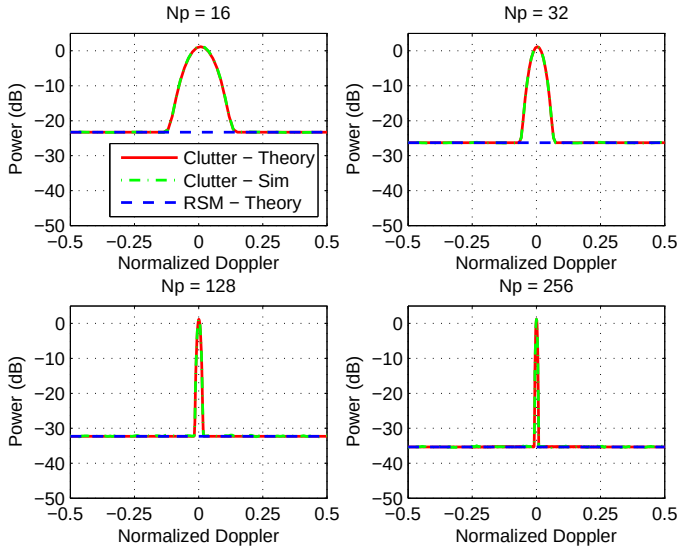

Fig. 3. Clutter power computed via (8), by simulation, and RSM power computed via (9) plotted as a function of the normalized Doppler frequency ϕ for $N_p = 16, 32, 128$ and 256 pulses per CPI.

will be very tight for $|\phi| \geq \overline{\phi}$. For any target associated with a normalized Doppler frequency greater than $\overline{\phi}$, i.e. $\phi_{\text{trg}} \geq \overline{\phi}$, the detection performance will strongly depend on the RSM power (the right hand side of the inequality in (9)), denoted as $RSM_{\text{POWER}}(\mathbf{\Gamma}, h, \sigma_\omega^2, N_p, N_c, N_r)$. Note that for a target echo with power P_r at normalized Doppler frequency ϕ_{trg} (the target return in the n_p-th PRI is $\sqrt{P_r}\exp\{j2\pi\phi_{\text{trg}}n_p\}\, s_{n_p}(t;\boldsymbol{\beta},\boldsymbol{\alpha}_{n_p})$), the peak signal power after MF-DFT processing (without straddling losses) is P_r. Unlike the RSM power, the peak signal power does not depend on the parameters $\mathbf{\Gamma}, h, \sigma_\omega^2, N_p, N_c$, and N_r. The signal-to-clutter ratio (SCR) is defined as P_r/σ_ω^2. The SCR is a measure of the relative strength of the (peak) target echo power to the peak clutter power after MF-DFT processing, which occurs at zero Doppler and—for small h, and large N_c and N_r—is approximately equal to $4\sigma_\omega^2/3$.

It can be shown that the term $\sin^2(h\pi)\left(1+\cos^2(h\pi)\right)$, and hence the RSM power, is a decreasing function of h on $(0, \frac{1}{2}]$. For $h \ll \frac{1}{2}$, the small angle approximation (i.e. $\sin(x) \approx x$, and $\cos(x) \approx 1$) can be invoked, resulting in $\sin^2(h\pi)\left(1+\cos^2(h\pi)\right) \approx 2h^2\pi^2$. Therefore, for small values of h, reducing h by a factor of 2 results in approximately a 6 dB reduction in the RSM power. The strong dependence on h stems from the fact that REC waveforms become more similar, and thus the MF range sidelobes become more coherent, as h is reduced. The term $\sum_{n_p=0}^{N_p-1}\Gamma_{n_p}^2$ encapsulates the dependence of the RSM power on both N_p and $\mathbf{\Gamma}$. For a given type of Doppler windowing function (e.g. Hamming, Taylor, etc.), and given the normalization $\sum_{n_p=1}^{N_p-1}\Gamma_{n_p} = 1$, this term can be written as the product of $1/N_p$ and a *Doppler windowing loss* term—with respect to the rectangular Doppler windowing function—which does not significantly vary with N_p [28]. The reduction in RSM power achieved by increasing the number of pulses is analogous to the radar receiver SNR processing gain. The terms in the clutter return that give rise to the RSM power component are zero-mean and i.i.d. across the pulses of the CPI, like the additive white Gaussian noise (AWGN) samples at the radar receiver. The dependence on the sampling rate N_r is weak since setting $N_r \geq 2$ results in $\frac{2}{3} < \frac{2}{3} + \frac{1}{3N_r^2} \leq \frac{3}{4}$. The dependence on the time-bandwidth product N_c is also weak since practical values of N_c lead to $\frac{N_c-1}{N_c} \approx 1$. Lastly, the RSM power linearly scales with the clutter power parameter σ_ω^2, which is expected as higher clutter power simply leads to higher residual clutter.

IV. Numerical Results

In Fig. 2 the theoretical clutter power computed via (8), by simulation, and the theoretical RSM power computed via (9) are shown as a function of the normalized Doppler frequency ϕ for modulation indices $h = \frac{1}{2}, \frac{1}{8}, \frac{1}{32}$ and $\frac{1}{128}$. The remaining parameter values are $\sigma_\omega^2 = 1$, $N_p = 64$, $N_c = 64$, and $N_r = 4$. The DFT is computed with a Taylor window having a -55 dB peak-to-sidelobe ratio. It is observed that the theoretical clutter power and the clutter power computed by simulation match for all h values, which is expected because the clutter model used for simulations is the same model used in the derivation of (8). In addition, the theoretical RSM power (dashed blue line) establishes a very tight lower bound on the clutter power. Finally, it is observed that the RSM power decreases by approximately 12 dB when h is divided by 4, as predicted by the theoretical analysis.

In Fig. 3 the same three quantities are illustrated for $N_p = 16, 32, 128$ and 256 pulses per CPI. The modulation index is fixed as $h = \frac{1}{16}$, and all other parameters are the same as those used for Fig. 2. It is observed that the RSM power decreases by 3 dB (6 dB) as N_p is reduced by a factor of 2 (4), which is also consistent with the theoretical analysis. We emphasize

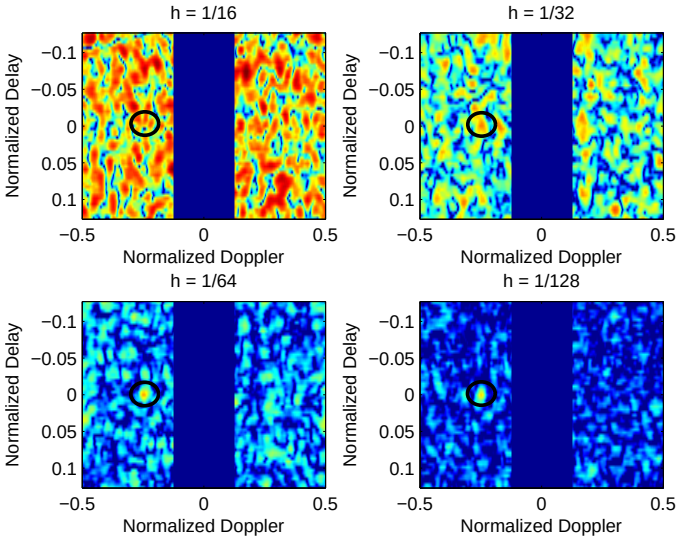

Fig. 4. The range-Doppler response (dB) to a point target (black circle) located at normalized Doppler frequency $\phi = -\frac{1}{4}$ and normalized delay 0 for modulation indices $h = \frac{1}{8}, \frac{1}{16}, \frac{1}{64}$ and $\frac{1}{128}$, with $N_p = 64$.

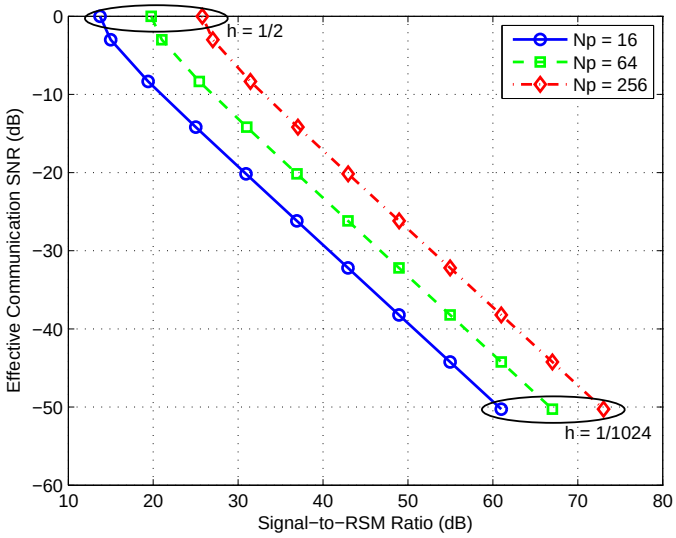

Fig. 5. Normalized effective communication SNR vs. normalized signal-to-RSM ratio as a function of h ($h = \frac{1}{2}, \frac{1}{4}, \cdots, \frac{1}{1024}$) for $N_p = 16, 64$ and 256 pulses per CPI.

that the peak signal power for a given target after MF-DFT processing does not depend on h or N_p. Therefore, if a target echo having power P_r (SCR of $\frac{1}{P_r}$ from $\sigma_\omega^2 = 1$) is included in Figures 2 and 3, it would have the same peak power in all eight plots.

In Fig. 4 the range-Doppler response (dB) to a point target positioned at the normalized Doppler frequency $\phi_{\text{trg}} = -\frac{1}{4}$ and normalized delay 0 is shown for modulation indices $h = \frac{1}{16}, \frac{1}{32}, \frac{1}{64}$ and $\frac{1}{128}$. The number of pulses per CPI is $N_p = 64$, the clutter power parameter is $\sigma_\omega^2 = 30$ dB and the peak target return power is $P_r = 0$ dB (i.e. the SCR is -30 dB). The clutter-to-noise ratio (CNR) is $\sigma_\omega^2/\sigma_\eta^2 = 50$ dB, where σ_η^2 is the variance of additive Gaussian noise after MF-DFT processing without windowing. An ideal "brickwall" high-pass filter is used to cancel the clutter response at the normalized Doppler values $\phi \in [-0.1, 0.1]$. The biphase radar code of length $N_c = 65$ is obtained by the Kronecker product of a length-13 and a length-5 Barker code as described in [29]. The remaining parameters, have the same values as those used for Figures 2 and 3. The target location is indicated by a black circle. It is observed that the target visibility is enhanced by reducing the modulation index since the target is slightly brighter than the response at the surrounding range-Doppler bins for $h = \frac{1}{64}$, and much brighter for $h = \frac{1}{128}$. For these cases, the signal-to-RSM ratio (defined in (10)) is 11.2 dB and 17.2 dB, respectively.

Finally, REC system operating curves are presented to illustrate the relationship between the SNR at the communication receiver and the signal-to-RSM ratio (S-RSM) at the radar receiver as a function of the modulation index h. The S-RSM is defined as the ratio of the peak target echo power to the RSM power, or

$$\text{S-RSM} = \frac{P_r}{RSM_{\text{POWER}}(\mathbf{\Gamma}, h, \sigma_\omega^2, N_p, N_c, N_r)}. \quad (10)$$

Since the clutter power for normalized Doppler values greater than some threshold is tightly approximated by the RSM power, the signal-to-RSM ratio quantifies the effective clutter interference power from a moving target indication (MTI) point of view. In Fig. 5 three curves are generated, each with modulation indices $h = \frac{1}{2}, \frac{1}{4}, \cdots, \frac{1}{1024}$, for $N_p = 16, 64$ and 256 pulses per CPI. The Doppler windowing function is rectangular, and the over-sampling is $N_r = 4$. The horizontal axis represents the *normalized S-RSM* (dB) and the vertical axis represents the *normalized effective SNR* at the communication receiver (dB). The normalized S-RSM is computed by setting P_r/σ_ω^2 to unity in (10). For a given negative value of $P_r/\sigma_\omega^2(\text{dB}) = -X(\text{dB})$, the respective system operating curves can be obtained by shifting the curves in Fig. 5 to the left by $X(\text{dB})$.

From a communication system perspective, the PSK modulation under consideration for a given SNR value E_b/N_0, where E_b is the energy per bit and N_0 is the (one-sided) AWGN power spectral density at the communication receiver, is equivalent to binary PSK (BPSK) with an SNR of $\sin(h\pi)^2 \frac{E_b}{N_0}$ [26]. This BPSK-equivalent SNR is referred to as the effective SNR, and the normalized effective SNR is obtained by setting $\frac{E_b}{N_0} = 1$. For a given positive value of $\frac{E_b}{N_0} = Y(\text{dB})$ the respective system operating curves can be obtained by shifting the curves in Fig. 5 upward by $Y(\text{dB})$. The modulation index $h = \frac{1}{2}$ leads to the best case scenario from a communication perspective (the SNR is equal to the effective SNR), while it leads to the worst case scenario from a radar perspective. Because the communication SNR is not a function of N_p, increasing/decreasing N_p shifts the

system operating curves to the right/left. According to Fig. 5, a significant increase in the signal-to-RSM ratio can only be achieved by a significant reduction in the effective communication SNR. However, radar transmitters tend to operate at high power and the attenuation between the radar transmitter and communication receiver at distance R is proportional to $\frac{1}{R^2}$. Hence, in most cases satisfactory communication system performance can be achieved even with small values of h. If the effective communication SNR prevents satisfactory communication performance, channel coding can also be employed to trade-off data throughput for lower probability of decoding error [30], [31].

V. Conclusions and Future Work

A closed-form expression for the power of the residual clutter occurring in coding diversity REC was derived for a phase-modulated system. The residual clutter power, referred to as the range sidelobe modulation (RSM) power, is not a function of the normalized Doppler frequency, and thus establishes a clutter interference floor in the clutter range-Doppler response. In addition, RSM is approximately quadratic with the modulation index and inversely proportional to the number of pulses in the CPI, but it does not vary appreciably with the radar code length. The theoretical results were validated by simulation and the RSM power expression was used to generate REC system operating curves illustrating the trade-off between the SNR at the communication receiver and the signal-to-RSM ratio at the radar receiver.

Ongoing work is generalizing this analysis to other waveform structures, for arbitrary values of the number of communication symbols per pulse, and the number of bits per communication symbol. In addition, a more general clutter model is being investigated to allow for spatial correlation as well as variation from pulse to pulse within a CPI.

References

[1] H. Griffiths, L. Cohen, S. Watts, E. Mokole, C. Baker, M. Wicks, and S. D. Blunt, "Radar spectrum engineering and management: Technical and regulatory issues," *Proceedings of the IEEE*, vol. 103, pp. 85–102, Jan 2015.

[2] Strategic Technology Office and Defense Advanced Research Projects Agency, *Shared Spectrum Access for Radar and Communications (SSPARC)*. [Online]. Available: http://www.darpa.mil/program/shared-spectrum-access-for-radar-and-communications, accessed Jan. 2016.

[3] M. Wicks, E. Mokole, S. Blunt, R. Schneible, and V. Amuso, eds., *Principles of Waveform Diversity and Design*. Raleigh, NC: SciTech Publishing, 2010.

[4] S. Pillai, K. Y. Li, and B. Himed, *Waveform Diversity: Theory & Applications*. McGraw-Hill, 2011.

[5] S. D. Blunt and E. L. Mokole, "Overview of radar waveform diversity," *IEEE Aerospace and Electronic Systems Magazine*, vol. 31, pp. 2–42, November 2016.

[6] S. D. Blunt, M. R. Cook, and J. Stiles, "Embedding information into radar emissions via waveform implementation," *International Waveform Diversity and Design Conference*, pp. 195–199, Aug. 2010.

[7] C. Sahin, J. Jakabosky, P. M. McCormick, J. G. Metcalf, and S. D. Blunt, "A novel approach for embedding communication symbols into physical radar waveforms," *IEEE Radar Conference*, May 2017.

[8] M. J. Nowak, Z. Zhang, Y. Qu, D. A. Dessources, M. Wicks, and Z. Wu, "Co-designed radar-communication using linear frequency modulation waveform," *IEEE Military Communications Conference*, pp. 918–923, Nov. 2016.

[9] X. Chen, X. Wang, S. Xu, and J. Zhang, "A novel radar waveform compatible with communication," *International Conference on Computational Problem-Solving*, pp. 177–181, Oct. 2011.

[10] C. Sturm and W. Wiesbeck, "Waveform design and signal processing aspects for fusion of wireless communications and radar sensing," *Proceedings of the IEEE*, vol. 99, pp. 1236–1259, July 2011.

[11] A. Hassanien, M. G. Amin, Y. D. Zhang, and F. Ahmad, "Dual-function radar-communications: information embedding using sidelobe control and waveform diversity," *IEEE Transactions on Signal Processing*, vol. 64, pp. 2168–2181, Apr. 2016.

[12] J. G. Metcalf, C. Sahin, S. D. Blunt, and M. Rangaswamy, "Analysis of symbol-design strategies for intrapulse radar-embedded communications," *IEEE Transactions on Aerospace and Electronic Systems*, vol. 51, pp. 2914–2931, Oct. 2015.

[13] Y. Huang, M. Piezzo, V. Carotenuto, and A. De Maio, "Radar waveform design under similarity, bandwidth priority, and spectral coexistence constraints," *IEEE Radar Conference*, May 2017.

[14] M. Mehrnoush and S. Roy, "Interference mitigation in coexistence of wlan network with radar," *IEEE Radar Conference*, May 2017.

[15] A. Chiriyath, B. Paul, and D. Bliss, "Simultaneous radar detection and communications performance with clutter mitigation," *IEEE Radar Conference*, May 2017.

[16] B. Ravenscroft, P. M. McCormick, S. D. Blunt, J. Jakabosky, and J. G. Metcalf, "Tandem-hopped OFDM communications in spectral gaps of FM noise radar," *IEEE Radar Conference*, May 2017.

[17] P. M. McCormick, S. D. Blunt, and J. G. Metcalf, "Simultaneous radar and communication emissions from a common aperture, part i: theory," *IEEE Radar Conference*, May 2017.

[18] A. C. O'Connor, J. M. Kantor, and J. Jakabosky, "Joint equalization filters that mitigate waveform-diversity modulation of clutter," *IEEE Radar Conference*, May 2016.

[19] M. Cook, S. D. Blunt, and J. Jakabosky, "Optimization of waveform diversity and performance for pulse-agile radar," *IEEE Radar Conference*, May 2011.

[20] D. Scholnik, "Range-ambigious clutter suppression with pulse-diverse waveforms," *IEEE Radar Conference*, pp. 336–341, May 2011.

[21] T. Higgins, S. D. Blunt, and A. K. Shackelford, "Time-range adaptive processing for pulse agile radar," *International Waveform Diversity and Design Conference*, pp. 115–120, Aug. 2010.

[22] T. Higgins, K. Gerlach, A. K. Shackelford, and S. D. Blunt, "Aspects of non-identical multiple pulse compression," *IEEE Radar Conference*, pp. 895–900, May 2011.

[23] C. Sahin, J. G. Metcalf, and S. D. Blunt, "Filter design to address range sidelobe modulation in transmit-encoded radar-embedded communications," *IEEE Radar Conference*, May 2017.

[24] S. D. Blunt, M. R. Cook, J. Jakabosky, J. De Graaf, and E. Perrins, "Polyphase-coded FM (PCFM) radar waveforms, part i: implementation," *IEEE Transactions on Aerospace and Electronic Systems*, vol. 50, pp. 2218–2229, July 2014.

[25] J. B. Anderson, T. Aulin, and C.-E. Sundberg, *Digital Phase Modulation*. New York: Plenum Press, 1986.

[26] J. G. Proakis, *Digital Communications*. New York: McGraw-Hill, 2008.

[27] P. S. Tan, J. Jakabosky, J. M. Stiles, and S. D. Blunt, "On higher-order representations of polyphase-coded fm radar waveform," *IEEE Radar Conference*, May 2015.

[28] M. A. Richards, J. A. Scheer, and W. Holm, *Principles of Modern Radar, Vol. I: Basic Principles*. Raleigh, NC: SciTech Publishing, 2010.

[29] M. A. Richards, *Fundamentals of Radar Signal Processing*. New York City, NY: McGraw-Hill Education, 2014.

[30] Y. Polyanskiy, H. Poor, and S. Verdu, "Channel coding rate in the finite blocklength regime," *IEEE Transactions on Information Theory*, vol. 56, pp. 2307–2359, May 2010.

[31] C. Sahin, L. Liu, and E. Perrins, "On the queueing performance of HARQ systems with coding over finite transport blocks," *IEEE Globecom Workshop on Ultra-Low Latency and Ultra-High Reliability in Wireless Communications*, Dec. 2015.